Volume 14 | Number 43 | 21 November 2018 | Pages 8675–8862

Soft Matter

rsc.li/soft-matter-journal

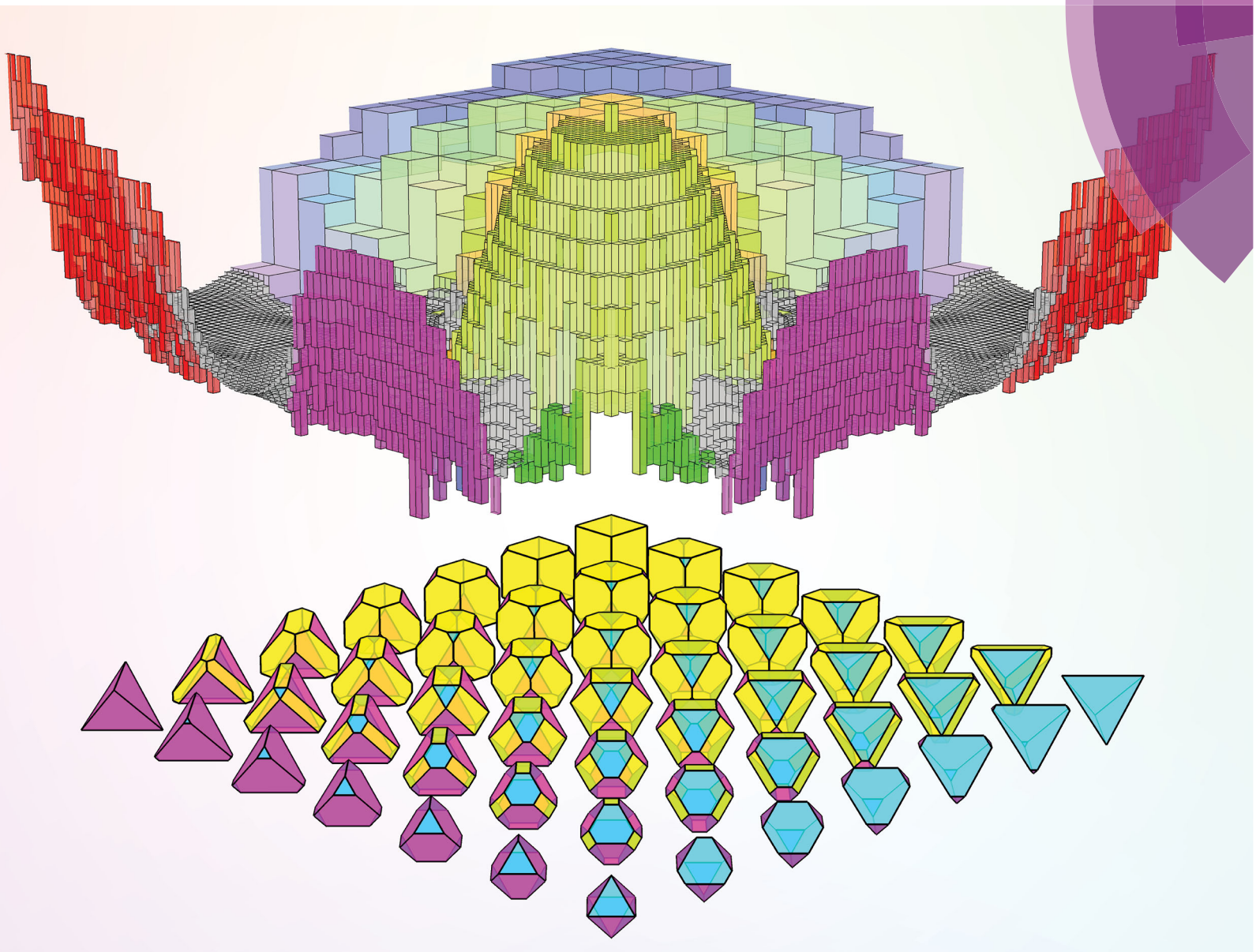

ISSN 1744-6848

ROYAL SOCIETY OF CHEMISTRY

PAPER
Daphne Klotsa, Sharon C. Glotzer *et al.*
Intermediate crystalline structures of colloids in shape space

Soft Matter

PAPER

Cite this: *Soft Matter*, 2018, **14**, 8692

Intermediate crystalline structures of colloids in shape space

Daphne Klotsa,†*[ab] Elizabeth R. Chen,†[ac] Michael Engel[ad] and Sharon C. Glotzer*[aef]

Received 1st August 2018,
Accepted 16th August 2018

DOI: 10.1039/c8sm01573b

rsc.li/soft-matter-journal

We computationally study the thermodynamic assembly of more than 40 000 hard, convex polyhedra belonging to three families of shapes associated with the triangle groups 323, 423, and 523. Each family is defined by vertex and/or edge truncation of symmetric polyhedra with equal edge length, producing shapes for which the majority are intermediates of more symmetric polyhedra found among the Platonic, Archimedean, and Catalan solids. In addition to the complex crystals cI16 lithium, BC8 silicon, γ-brass, β-manganese, and a dodecagonal quasicrystal, we find that most intermediate shapes assemble distorted variants of four basic cubic crystals: face-centered cubic, body-centered cubic, simple cubic, and diamond. To quantify the degree of distortion, we developed an algorithm that extracts lattice vectors from particle positions and then evaluates closeness to the four reference cubic crystals. This analysis allows us to group together in shape space related intermediate structures that would otherwise be placed in different lattice systems had we followed the lattice systems' strict definitions for angles and lengths of lattice vectors. The resulting landscapes show, as a function of shape, regions where ordered structures assemble, what is assembled and at what density, locations of transitions between regions of ordered structures, and regions of disorder. Our results provide a guide to self-assembling a host of related colloidal crystals through systematic design, by careful tweaking of the particle shape.

I. Introduction

With the growing interest in assembling colloidal crystals from nanometer- to micron-sized particles for a host of applications, it is important to understand how particle attributes relate to the thermodynamically stabilized crystals into which the particles assemble.[1–10] Computer simulations now easily allow studies of families of continuously related shapes, permitting the discovery of trends in crystal structure as particle shape is varied smoothly and systematically. In one-parameter families of shapes, the shape is varied between two ends of commonly known symmetric shapes. Examples include bowls where the thickness of the bowl is varied,[11] superballs that interpolate between a cube and an octahedron *via* a sphere,[6,12,13] polyhedra interpolating between a tetrahedron and an octahedron,[4] and polyhedra interpolating between a cube and an octahedron.[7] All these works predict crystal structures that change as a function of particle shape. Unlike atoms, colloidal particles do not obey charge quantization, and thus intermediate structures are not only possible, but expected. Intermediate shapes between the two ends of the interpolation between regular shapes assemble structures that have been reported as distorted versions of basic crystals.[7,12,13] It is these distorted structures we focus on, here. We argue that understanding distorted – or, as we shall call them, intermediate – structures is important because (i) they are abundant, as we will show; (ii) they may be relevant for experiments, as experimentally synthesized shapes may be intermediate shapes; (iii) they may have interesting macroscopic properties in their own right, opening up the parameter space for materials; (iv) they may be useful for gaining insight into structural transitions as a function of shape; and (v) they can be useful for designing glass-forming shapes that do not assemble any ordered structure.

In this paper, we computationally studied the thermodynamic assembly of tens of thousands of hard, symmetric, convex polyhedra that belong to three families of continuously modified shapes. We quantified the degree of distortion of colloidal crystal structures, assembled by intermediate shapes, by introducing an

[a] *Department of Chemical Engineering, University of Michigan, Ann Arbor, Michigan, 48109, USA. E-mail: sglotzer@umich.edu*
[b] *Department of Applied Physical Sciences, University of North Carolina, Chapel Hill, North Carolina 27599, USA. E-mail: dklotsa@email.unc.edu*
[c] *School of Engineering and Applied Sciences, Harvard University, Cambridge, MA, USA*
[d] *Institute for Multiscale Simulation, Friedrich-Alexander University Erlangen-Nürnberg, 91052 Erlangen, Germany*
[e] *Department of Materials Science and Engineering, University of Michigan, Ann Arbor, Michigan, 48109, USA*
[f] *Biointerfaces Institute, University of Michigan, Ann Arbor, Michigan 48109-2136, USA*
† D. K. and E. R. C. contributed equally to this work.

algorithm that extracted lattice vectors from particle positions and evaluated the similarity of the intermediate structure to four reference crystals: face-centered cubic (FCC), body-centered cubic (BCC), simple cubic (SC), and diamond (DIA). This analysis allowed us to group together in shape space related structures that would otherwise be placed in different lattice systems (triclinic, monoclinic, orthorhombic, tetragonal, hexagonal, cubic) had we followed the lattice systems' strict definitions for angles and lengths of lattice vectors. Our results are presented as "assembly landscapes" – surfaces of the minimum density for self-assembly *vs.* shape parameters – that reveal regions in shape space where ordered structures assemble, locations of transitions between ordered structures, and regions of disorder. We found that the minimum assembly density systematically increases towards the edges of regions of order, indicating a tendency towards decreasing thermodynamic stability of the ordered phase relative to that of the disordered fluid. In addition to distorted crystal structures, we found complex crystal structures in isolated regions of shape space. These structures include cI16 lithium (Li), γ-brass, β-manganese (Mn), a dodecagonal quasicrystal (QC), and, here reported for the first time, BC8 silicon (Si). We conclude by comparing our assembly landscapes to previously reported putative densest packing landscapes evaluated for the same three shape families.[14]

II. Model and methods

A. Shape families

We studied three families of shapes that have tetrahedral symmetry (triangle group 323), octahedral/cubic symmetry (triangle group 423), and icosahedral/dodecahedral symmetry (triangle group 523), as in ref. 14, see Fig. 1a–c. Polyhedra are constructed by applying edge truncation and/or vertex truncation to all five Platonic solids defining three domains of two-parameter shape families with parameters $0 \leq a, c \leq 100$ (Fig. 1a–c). The most regular polyhedra are found in the four corners of each domain. For family 323 (Fig. 1a), clockwise from top left is the tetrahedron, cube, tetrahedron, and octahedron. For family 423 (Fig. 1b), clockwise from top left is the cube, rhombic dodecahedron, octahedron, and cuboctahedron. For the family 523 (Fig. 1c), clockwise from top left is the dodecahedron, rhombic triacontahedron, icosahedron, and icosidodecahedron. Note that in the 323 family only, there is symmetry about the diagonal $a = c$ (connecting the cube and octahedron), so $\langle a, c\rangle = \langle c, a\rangle$ and all properties are symmetric about that diagonal. Some other regular polyhedra are found in the interior; these include the cuboctahedron at $\langle a, c\rangle = \langle 50, 50\rangle$ in the 323 family, Fig. 1a, truncated octahedron that tiles space at $\sim \langle 0, 20\rangle$ in the 323 family, Fig. 1b, and truncated icosahedron, also known as the buckyball at $\sim \langle 25, 0\rangle$ in the 523 family, Fig. 1c.

B. Self-assembly simulations

We performed isochoric Monte-Carlo (MC) simulations in shape-fluctuating boxes as in ref. 1, 4 and 5. Shapes were defined as hard particles with only steric interactions. Potential overlaps between polyhedra were identified through the Gilbert–Johnson–Keerthi algorithm[15] and discarded. Each simulation contained $N = 2000$ particles in a periodic box initiated from an equilibrated fluid phase at packing fraction (density) $\phi = 0.4$. Most of the simulations spontaneously crystallized at densities $0.5 \leq \phi \leq 0.64$ within 5×10^6 MC steps. If a simulation did not crystallize within this time limit, we extended the run for another 200×10^6 MC steps. If still no crystal was observed within the second time limit, the system was labeled "disordered." We initially ran four independent simulations with different initializations for each shape in a parameter grid of 21×21 (441 shapes per family). In regions of shape space where we observed many different crystal structures in close proximity, we refined the search grid further, *e.g.*, for the tetrahedral family, for $a, c \leq 34$, we refined to a grid of 101×101 (40 804 simulations).

C. Structure identification

Initial structure identification was performed using bond orientational order diagrams (BODs). BODs are histograms of the directions of bonds connecting a particle to its nearest neighbors projected onto the surface of a unit sphere.[16,17] Clear peaks indicate a well-formed crystal, and structurally distinct crystals yield different BODs. Disordered systems have isotropic BODs with no peaks. By construction, most of the shapes investigated here are intermediates between more regular polyhedra that define the boundaries (corners) of our shape space. Assemblies have been reported previously for these regular (corner) shapes[1,4,5,18] and for a one-parameter 432 subfamily,[7] and those results are confirmed here. For the intermediate shapes in our families, the BODs frequently appeared as distorted variants of the high-symmetry patterns that we typically observe for the regular shapes. We therefore require a more sophisticated method to quantify the distortion (shear) of the crystal unit cells.

D. Similarity to reference crystal structures

We assert that many of the crystals assembled here with distorted BODs are more usefully viewed as distorted/sheared versions of cubic reference crystal structures, *i.e.* intermediates. To analyze this relationship, we extracted basis vectors from particle simulation data that assembled periodic structures and then quantified how close the data were to reference crystals: SC, BCC, FCC, and DIA.[19]

1. Unit cell extraction. Starting from a set of N particle positions $\{\boldsymbol{r}_n\}$, we analyze the peak positions of the structure factor

$$S(\boldsymbol{q}) = \frac{1}{N}\left|\sum_{n=1}^{N} \exp(i\boldsymbol{q}\cdot\boldsymbol{r}_n)\right|^2$$

taking into account symmetry, extinction and interference effects. Given a reference crystal structure, we select a set of M diffraction peaks $\{(h_m k_m \ell_m)\}$ and search for a basis in reciprocal space $\{\boldsymbol{b}_1, \boldsymbol{b}_2, \boldsymbol{b}_3\}$ that maximizes

$$\nu = \sum_{m=1}^{M} S(h_m\boldsymbol{b}_1 + k_m\boldsymbol{b}_2 + \ell_m\boldsymbol{b}_3).$$

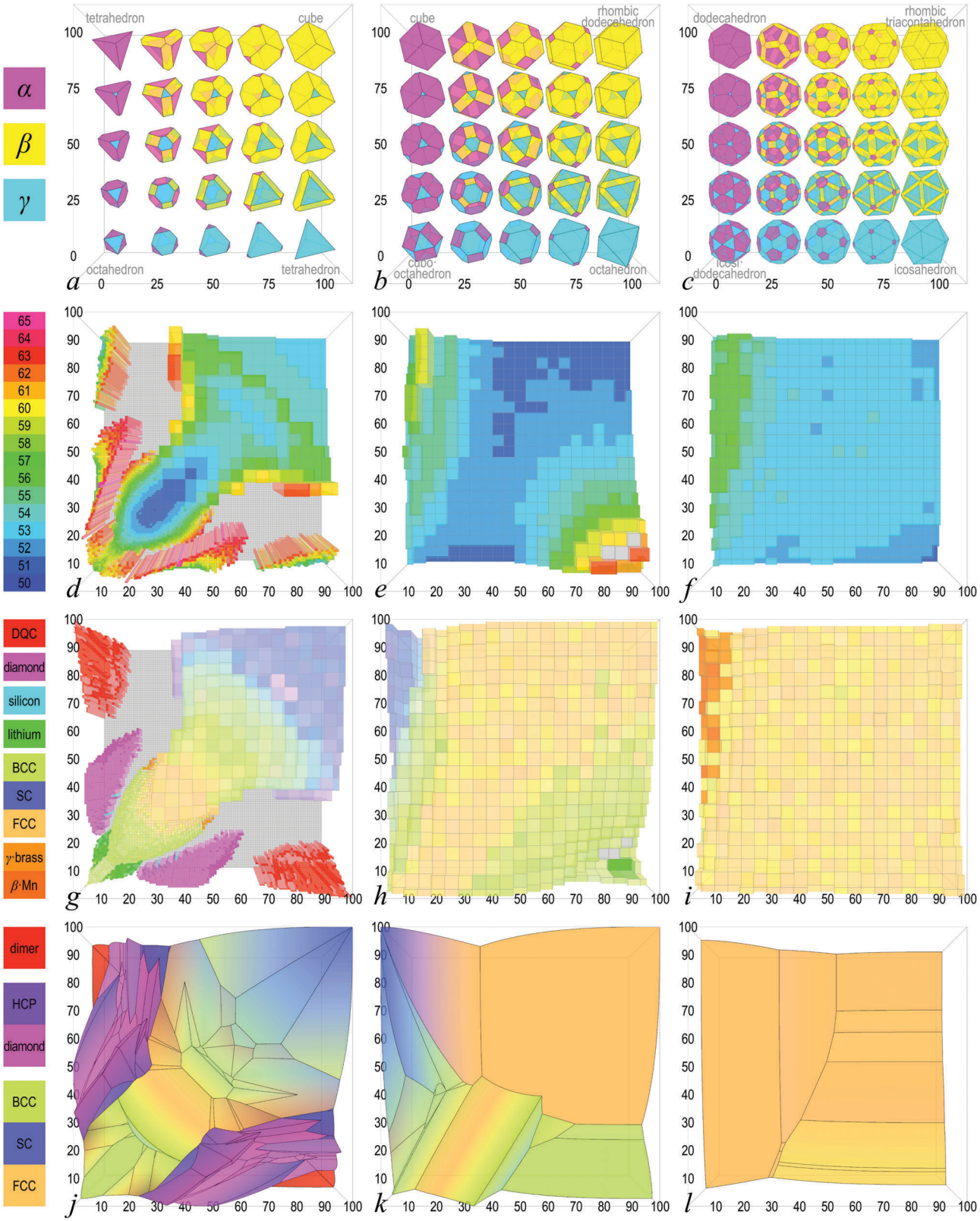

Fig. 1 Landscapes in shape space for minimum density for self-assembly, self-assembled crystal structure, and putative densest packings. Columns: shape family 323 (a, d, g and j), 423 (b, e, h and k), 523 (c, f, i and l). Rows: shapes (a–c), minimum assembly density (d–f), self-assembled structure (g–i), putative densest packing structure (j–l). In (d–f) height indicates minimum assembly density; in (g–i) height is inverted to aid the eye.

Specifically, we use $M_{SC} = 6$, $M_{BCC} = 12$, $M_{FCC} = 8$, $M_{DIA} = 4$ diffraction peaks allowed by selection rules,

$$\{(hk\ell)\}_{SC} = \{\langle 200\rangle\},$$

$$\{(hk\ell)\}_{BCC} = \{\langle 110\rangle\},$$

$$\{(hk\ell)\}_{FCC} = \{\langle 111\rangle\},$$

$$\{(hk\ell)\}_{DIA}{}^{+} = \{\langle 111\rangle : hk\ell = +1\},$$

$$\{(hk\ell)\}_{DIA}{}^{-} = \{\langle 111\rangle : hk\ell = -1\}.$$

Note that the choices $\{(hk\ell)\}_{DIA}{}^{+}$ and $\{(hk\ell)\}_{DIA}{}^{-}$ lead to identical quantifications, but we list both for symmetry. In our algorithm, the search is performed by testing 10^6 random values for the reciprocal lattice basis. From each reciprocal lattice basis of a reference crystal structure, we obtain the corresponding lattice basis $\{\zeta,\xi,\varsigma\}$ in real space.

2. Color map. We quantify how similar the obtained lattice bases are to those of the reference crystal structures. For this purpose, we measure orthogonality of vector angles,

$$\lambda_{point}^{angle} = \frac{\det\{\zeta,\xi,\varsigma\}^{2/3}}{(\zeta^2,\xi^2,\varsigma^2)^{1/3}},$$

$$\lambda_{plane}^{angle} = \frac{\det\{\xi\times\varsigma,\varsigma\times\zeta,\zeta\times\xi\}^{2/3}}{((\xi\times\varsigma)^2(\varsigma\times\zeta)^2(\zeta\times\xi)^2)^{1/3}},$$

and equality of vector lengths,

$$\lambda_{point}^{length} = \frac{(\zeta^2,\xi^2,\varsigma^2)^{1/3}}{\frac{1}{3}(\zeta^2+\xi^2+\varsigma^2)},$$

$$\lambda_{plane}^{length} = \frac{\left((\xi\times\varsigma)^2+(\varsigma\times\zeta)^2+(\zeta\times\xi)^2\right)^{1/3}}{\frac{1}{3}((\xi\times\varsigma)^2+(\varsigma\times\zeta)^2+(\zeta\times\xi)^2)}$$

and combine them into

$$\lambda^{angle} = \lambda_{point}^{angle}\lambda_{plane}^{angle},$$

$$\lambda^{length} = \lambda_{point}^{length}\lambda_{plane}^{length},$$

$$\lambda = \lambda^{angle}\lambda^{length}.$$

Note that $\det\{\xi\times\varsigma,\varsigma\times\zeta,\zeta\times\xi\} = \det\{\zeta,\xi,\varsigma\}^2$. Similarity to reference crystal structures is measured by

$$\mu_{SC}\{\zeta,\xi,\varsigma\} = \lambda\{\zeta,\xi,\varsigma\},$$

$$\mu_{BCC}\{\zeta,\xi,\varsigma\} = \lambda\{\xi+\varsigma-\zeta,\varsigma+\zeta-\xi,\zeta+\xi-\varsigma\},$$

$$\mu_{FCC}\{\zeta,\xi,\varsigma\} = \lambda\{\xi+\varsigma,\varsigma+\zeta,\zeta+\xi\},$$

$$\mu_{DIA}\{\zeta,\xi,\varsigma\} = \lambda\{\xi+\varsigma,\varsigma+\zeta,\zeta+\xi\}.$$

We choose colors for the assembly landscapes and the previously reported putative densest packing landscapes using the following mapping onto the rgb color cube,

$$\langle \text{red,green,blue}\rangle = \langle(\mu_{FCC})^p,(\mu_{BCC})^p,(\mu_{SC})^p\rangle,$$

$$\langle \text{red,green,blue}\rangle = \langle(\mu_{DIA}^{angle})^q,0,(\mu_{DIA}^{length})^q\rangle,$$

where we set $p = 4$ and $q = 2$ for contrast and

$$\mu_4^{angle}\{\zeta,\xi,\varsigma\} = \lambda^{angle}\{\xi+\varsigma,\varsigma+\zeta,\zeta+\xi\},$$

$$\mu_4^{length}\{\zeta,\xi,\varsigma\} = \lambda^{length}\{\xi+\varsigma,\varsigma+\zeta,\zeta+\xi\}.$$

By the end of this analysis, we have reduced a high dimensional space to a single color that simultaneously tracks changes of magnitudes and/or angles of the lattice vectors for all our assembled structures with up to two particles in the primitive unit cell.

III. Results

A. Assembly landscapes

We applied the algorithm and color map metric μ to the cubic structures FCC, BCC, SC, DIA and intermediate (distorted) versions of them. We separately identified crystals that had unit cells with more than two particles ($n > 2$) and the quasicrystal using BODs. The disordered regions, also identified by their BODs, were not further characterized. We thus obtained diagrams showing assembly structure as a function of the two shape parameters for each family (Fig. 1g–i).

In the 323 family, the intermediate cubic structures occurred primarily along and on either side of the diagonal that connects the cube and octahedron, and at and around the truncated octahedron $\sim\langle 0.20\rangle$, (Fig. 1g). Near the cube at $\langle 100, 100\rangle$, the algorithm identified intermediate structures related to SC. Moving along the diagonal (from the cube at the top right to the octahedron at the bottom left) there is a gradual but clear transition from SC to BCC to FCC, and then again to BCC near the corner at the octahedron at $\langle 0, 0\rangle$. We also observe a region that assembled DIA, including β-tin, which is a distorted version of the diamond structure. The structures with unit cells with $n > 2$ form a region of cI16 Lithium around $\sim\langle 0, 15\rangle$, a region of the dodecagonal quasicrystal around the tetrahedron $\sim\langle 0, 100\rangle$, as well as single points of BC8 silicon at $\langle 30, 10\rangle$ and β-manganese at $\langle 50, 22\rangle$. Regions of disorder were frequently found between structures that had different numbers n of particles in their primitive unit cells, the exceptions being BC8 silicon ($n = 8$) adjacent to DIA ($n = 2$) and β-manganese ($n = 20$) adjacent to FCC ($n = 1$).

In the 423 family, there are large regions of intermediate structures related to FCC and BCC, a smaller region of SC intermediate structures, and clear transitions between them (Fig. 1h). In contrast, the 523 family mostly assembled FCC intermediates. We observed a region of β-manganese and γ-brass for intermediate shapes near the left edge of the domain, near the dodecahedron.

We also plotted the minimum assembly density as a function of the shape parameters (Fig. 1d–f), where we defined the minimum assembly density as the lowest packing fraction for which we observed crystal formation. In the 323 family, the

minimum assembly density is lowest in the FCC region, 51–52%, higher for SC and BCC, 53–54%, and rapidly increased in all cases to greater than 60% as the disordered regions were approached from any structure (Fig. 1d). In the 423 family, the minimum assembly density was greater than 54% at the top left corner, as well as, along the left edge of the domain, where SC and BCC intermediates formed. We observed a large region where FCC intermediates formed at minimum assembly density between 51–52%. Towards the bottom right corner of the 423 landscape, the minimum assembly density increased as FCC-intermediates transitioned to BCC-intermediates, and peaked at 62% towards the edge of the disordered region and for cI16 Lithium (Fig. 1e). In the 523 family, most shapes assembled FCC intermediates at minimum assembly densities 51–52%, while on the upper left edge of the domain, where γ-brass and β-manganese formed, the minimum assembly densities increased to 56–57% (Fig. 1f).

As can be seen by comparing Fig. 1d–f with Fig. 1g–i, visual inspection of the minimum assembly density landscapes is all that is needed to identify regions of ordered structures and transitions between different structures, even without knowing the identity of the structures. Thus, structural signatures of the thermodynamic assemblies are reflected in the minimum assembly density, even though the two measurements are independent of one another.

B. Comparison to putative densest packing landscapes

We previously reported putative[20] densest packings for the three family of shapes studied here calculated through a combination of Monte Carlo simulations and analytic optimization.[14] Here, we applied the algorithm we used to identify intermediate structures in the assembly data to the putative densest packing data (Fig. 1g–l) to make a direct comparison. The solid lines indicate regions of packings according to contacts calculated previously[14] and are shown here for reference. Of course, there is no *a priori* reason why the crystal that self-assembles at moderate densities should generally be the same as the mathematically optimized packing. The former arises from entropy maximization, while the latter arises from minimization of the Gibbs free energy in the limit of infinite pressure.

In comparing visually the assembly and packing landscapes for each family, we observe a general correspondence between assembly and densest packing for the simplest crystal structures. For the more complex structures, the putative densest packings generally differ from the observed assemblies. Of most relevance to this work is that those structures identified as intermediate in the assembly landscapes and labeled *via* the proposed algorithm to reflect their similarity to the basic cubic crystals, match the corresponding putative densest packings of the structures they are most similar to. This observation demonstrates a major strength of our algorithm, in that it reveals potential relationships between assemblies and packings that could be missed otherwise.

IV. Discussion and conclusion

Through a large and comprehensive set of computer simulations, we studied the thermodynamic assemblies of tens of thousands of polyhedra, most of which are intermediate shapes that occur through edge and/or vertex truncations of more symmetric polyhedra. We identified the cubic crystals SC, BCC, FCC, and DIA, as well as intermediate (distorted) versions of them, and more complex crystals, including cI16 lithium, BC8 silicon, γ-brass, β-manganese, and a dodecagonal quasicrystal. We presented an algorithm that identifies and accurately quantifies regions of intermediate crystal structures with reference to basic cubic crystals. The application of our algorithm to colloidal crystal assembly opens up new possibilities for designing materials properties that depend on targeting crystal structures having a given similarity to one of these reference structures.

As with previous works on packing, our structure and minimum assembly density landscapes can guide experiments and theory by serving as ''phase diagrams for shape'' – locating regions where crystals form, regions where crystals fail to form, and transitions between regions. For example, within regions that assemble crystals, our landscapes show how sensitive (or insensitive) the assembly of a crystal in a given region is to small variations in particle shape. For example, there are regions where small shape variations merely affect the assembled structure, such as near the cube in 323, and 423 families, or most shapes in the 523 family (forming FCC). Also, because experimentally synthesized shapes may deviate from perfect polyhedra, such knowledge is useful to evaluate how accurately the shape must be synthesized to achieve successful assembly. For example, in the 323 family the region of shape space over which the cI16 lithium structure forms is much smaller than the region over which BCC forms (Fig. 1g), implying that to assemble the cI16 lithium structure, shape synthesis must be more precise. The minimum assembly density landscapes also provide guidance in selecting shapes for synthesis. For example, to assemble FCC it may be advisable to use the shape with the lowest minimum assembly density shown in the interior of the FCC region, 50%, than a shape at the edge of the FCC region where the minimum assembly density can be as high as 60%. Already studies have used our landscapes to, *e.g.*, quantify solid–solid transitions in shape space[21] and determine why shapes in the disordered regions fail to assemble crystals.[22] Furthermore, the correspondence we observe between two independent measures of a crystal assembled from a given shape – namely, our algorithm's structure identification and the minimum density for self assembly – indicates a connection between them that should be further investigated in future work.

Conflicts of interest

There are no conflicts to declare.

Acknowledgements

D. K. acknowledges the FP7 Marie Curie Actions of the European Commission, Grant Agreement No. PIOF-GA-2011-302490 Actsa. D. K. would like to thank Angie Kehagia for helpful discussions. E. R. C. acknowledges the National Science Foundation, MSPRF DMS-1204686. This work was partially supported by a Simons

Investigator award from the Simons Foundation to S. C. G. This research was supported in part through computational resources and services supported by Advanced Research Computing at the University of Michigan, Ann Arbor.

References

1 A. Haji-Akbari, M. Engel, A. S. Keys, X. Zheng, R. G. Petschek, P. Palffy-Muhoray and S. C. Glotzer, Disordered, quasicrystalline and crystalline phases of densely packed tetrahedra, *Nature*, 2009, **462**, 773–777.

2 U. Agarwal and F. A. Escobedo, Mesophase behaviour of polyhedral particles, *Nat. Mater.*, 2011, **10**, 230–235.

3 C. Avendaño and F. A. Escobedo, Phase behavior of rounded hard-squares, *Soft Matter*, 2012, **8**, 4675.

4 P. F. Damasceno, M. Engel and S. C. Glotzer, Crystalline assemblies and densest packings of a family of truncated tetrahedra and the role of directional entropic forces, *ACS Nano*, 2012, **6**, 609–614.

5 P. F. Damasceno, M. Engel and S. C. Glotzer, Predictive self-assembly of polyhedra into complex structures, *Science*, 2012, **337**, 453–457.

6 R. Ni, A. P. Gantapara, J. de Graaf, R. van Roij and M. Dijkstra, Phase diagram of colloidal hard superballs: from cubes via spheres to octahedra, *Soft Matter*, 2012, **8**, 8826.

7 A. P. Gantapara, J. de Graaf, R. van Roij and M. Dijkstra, Phase diagram and structural diversity of a family of truncated cubes: degenerate close-packed structures and vacancy-rich states, *Phys. Rev. Lett.*, 2013, **111**, 015501.

8 M. R. Khadilkar, U. Agarwal and F. A. Escobedo, Phase behavior of binary mixtures of hard convex polyhedra, *Soft Matter*, 2013, **9**, 11557.

9 M. R. Khadilkar and F. A. Escobedo, Heuristic rule for binary superlattice coassembly: mixed plastic mesophases of hard polyhedral nanoparticles, *Phys. Rev. Lett.*, 2014, **113**, 165504.

10 Y. Geng, G. van Anders and S. C. Glotzer, *via*, 2018, arXiv:1801.06219.

11 M. Marechal and M. Dijkstra, Phase behavior and structure of colloidal bowl-shaped particles: simulations, *Phys. Rev. E: Stat., Nonlinear, Soft Matter Phys.*, 2010, **82**, 031405.

12 Y. Zhang, F. Lu, D. van der Lelie and O. Gang, Continuous phase transformation in nanocube assemblies, *Phys. Rev. Lett.*, 2011, **107**, 135701.

13 L. Rossi, V. Soni, D. J. Ashton, D. J. Pine, A. P. Philipse, P. M. Chaikin, M. Dijkstra, S. Sacanna and W. T. M. Irvine, Shape-sensitive crystallization in colloidal superball fluids, *Proc. Natl. Acad. Sci. U. S. A.*, 2015, **112**, 5286–5290.

14 E. R. Chen, D. Klotsa, M. Engel, P. F. Damasceno and S. C. Glotzer, Complexity in surfaces of densest packings for families of polyhedra, *Phys. Rev. X*, 2014, **4**, 011024.

15 E. G. Gilbert, D. W. Johnson and S. S. Keerthi, A fast procedure for computing the distance between complex objects in three-dimensional space, *IEEE J. Rob. Autom.*, 1988, **4**, 193–203.

16 P. J. Steinhardt, D. R. Nelson and M. Ronchetti, Bond-orientational order in liquids and glasses, *Phys. Rev. B: Condens. Matter Mater. Phys.*, 1983, **28**, 784–805.

17 W. Lechner and C. Dellago, Accurate determination of crystal structures based on averaged local bond order parameters, *J. Chem. Phys.*, 2008, **129**, 114707.

18 B. A. Schultz, P. F. Damasceno, M. Engel and S. C. Glotzer, Symmetry considerations for the targeted assembly of entropically stabilized colloidal crystals *via* Voronoi particles, *ACS Nano*, 2015, **9**, 2336–2344.

19 We do not distinguish between FCC and hexagonal-close packed (HCP) structures.

20 We refer to these packings as ''putative'' densest packings because, with the exception of space-filling shapes, there are no analytical proofs that the densest packings found for any polyhedron are indeed the densest possible mathematically.

21 C. X. Du, G. van Anders, R. S. Newman and S. C. Glotzer, Shape-driven solid–solid transitions in colloids, *Proc. Natl. Acad. Sci. U. S. A.*, 2017, **114**, E3892–E3899.

22 E. G. Teich, G. van Anders and S. C. Glotzer, Identity crisis in alchemical space drives the entropic colloidal glass transition, under review.